Research Article

Application of smoothed particle hydrodynamics (SPH) for simulating various geotechnical problems

Mohammed Russedul Islam[1] · **Md. Aftabur Rahman**[2] · **Kimitoshi Hayano**[3]

Received: 3 December 2019 / Accepted: 29 February 2020 / Published online: 17 March 2020

Abstract
Geotechnical engineering is considered one of the oldest disciplines in civil engineering. To date, to extract hidden information, numerical simulations have been performed using the traditional grid-based numerical approach in the Eulerian framework. However, this may not capture some geotechnical engineering problems caused by the large deformations of geomaterials. Therefore, in this research, an attempt is made to develop a particle-based method using smoothed particle hydrodynamics (SPH), which has proven to be an effective option for modeling geomaterials, to solve these problems through running different sets of numerical simulations. The developed model is validated using some benchmark solutions and then two important geotechnical problems, namely the bearing capacity and seepage flow profiles, are simulated. The simulated results represent the actual scenario quite well. Also, the flow process in terms of the accumulated strain is evaluated at different times, with the model justifying the proposed approach for simulating geotechnical problems.

Keywords SPH · Soil–water coupling · Drucker–Prager model · Bearing capacity

1 Introduction

Geotechnical engineering is one of the main branches of civil engineering and its significance has been recognized since the early age of modern history. As the ultimate goal of any structural design is to transmit super structural loads to a firm soil layer, it is of primary importance to evaluate certain soil parameters, especially their index and engineering properties. Numerous research studies have been conducted to determine the properties of geomaterials and gain insights into soils under applied loads. Although reliable experimental facilities have been developed and perform quite well, it is time to develop an alternative approach for ascertaining these properties using numerical simulations and analyses which can extract their mechanics and gain insights into this phenomenon. The advent of computational facilities and recent rapid development of appropriate tools have enabled sophisticated numerical models to simulate practical problems [1]. To date, the finite element method (FEM) based on an Eulerian framework is considered the most efficient numerical tool used in different branches of engineering [2]. Its basic formulation requires discretizing the entire domain into small pieces which makes it a grid-based method. However, if there is a large deformation that severely distorts the mesh, an entire simulation will eventually blow up. Although some FEM developments found in technical writings incorporate arbitrary Lagrangian behaviors [3], they are not always capable of realistically simulating large deformation processes. In addition, the finite difference method (FDM) has been used in many applications, together with FEM, to capture

✉ Mohammed Russedul Islam, russed@ce.mist.ac.bd; Md. Aftabur Rahman, maftabur@cuet.ac.bd; Kimitoshi Hayano, hayano@ynu.ac.jp
| [1]Department of Civil Engineering, Military Institute of Science and Technology, Mirpur Cantonment, Dhaka, Bangladesh. [2]Department of Civil Engineering, Chittagong University of Engineering and Technology, Chattogram 4349, Bangladesh. [3]Graduate School of Urban Innovation, Yokohama National University, Yokohama, Japan.

the entire deformation process. However, the large deformation phenomena, moving frames, and the necessity of capturing free surface flow restrict the use of FDM in large deformation geotechnical problems [2]. The above discussion indicates the need to develop an alternative approach for analyzing large deformation geomechanical problems. Recently, particle-based method for improving the limitation of a FEM for capturing large deformations using the Lagrangian's nature to track the motion of each point was proposed [2]. Of various particle-based methods, the discrete element model (DEM) was developed in 1970 to simulate the behaviors of granular materials [4]. Although its discrete particle nature can reproduce different geotechnical engineering applications quite well, it is computationally expensive and has some shortcomings in formulating the coupled analysis. Moreover, specification of DEM parameters is somewhat ambiguous and reliable guidelines have not yet established [5]. Another important numerical tool is the material point method (MPM) which uses a background mesh behind the particle assembly [6] and is capable of reproducing different geotechnical applications considering both single-phase materials and coupled problems [7, 8]. However, distortions of the background mesh may restrict its use in many instances. Other tools, such as the finite volume method (FVM) and moving particle semi-implicit (MPS) approach, have been used in a few applications but their simulation results are not consistent. The SPH tool was developed in the late 1970s with the aim of solving astrophysical problems [9]. Its true particle nature with no connectivity makes it popular and robust while its formulation is easy and its solution algorithm straightforward [10]. Considering its capability for handling boundary particles, Lagrangian nature and simple formulation has attracted researchers in different branches of engineering to use it in fields such as fluid dynamics, viscous flow, wave over-topping and dam-break flooding [11–22]. Furthermore, its application has been extended to simulating landslide dynamics, slope failures, fluid–solid interactions and associated problems [5, 23–32] and, in the preceding cases which involve large deformations, it performs quite well for replicating real instances [33–36]. Therefore, given all SPH's positive attributes, its extension to simulating traditional geotechnical engineering problems is a breakthrough in numerical modeling.

Among various geotechnical engineering problems, the bearing capacity of soils is of crucial importance as the ultimate loads of any superstructure is transmitted to the sub-soil. Besides, seepage occurs for earth retaining structures and often leads to failure of the system. The SPH method can also be checked to simulate some geotechnical experiments. Notably, permeability and shear tests are very much crucial in geotechnical engineering. Therefore, considering the above scenario, this research aimed to develop an SPH tool considering elasto-plastic soil and soil–water coupling phenomenon. Afterward, the SPH was validated through known geotechnical engineering experiments, and finally, the bearing capacity and seepage phenomenon of the soils were quantitatively investigated. The methods used and findings obtained from this study are discussed in later sections.

2 Fundamentals of particle method: smoothed particle hydrodynamics (SPH)

The basic concept of the particle method is fully established in a SPH framework as any shape of the problem domain can be set in it because there is no connection among the particles. Each particle contains its own individual properties, i.e., mass, density, velocity, etc., which are updated from those of surrounding ones within a specific range using a smoothing kernel. Then, numerical integration is performed to update each particle's position and the simulation continues until the desired time or velocity is reached. The first step in SPH is the integral representation of a field function mathematically expressed as

$$f(x) = \int_{\Omega} f\left(x'\right)\left(x - x'\right)\mathrm{d}x' \tag{1}$$

where $f(x)$ is a function of the three-dimensional position vector (x) and $\left(x - x'\right)$ the Dirac delta function given by

$$\left(x - x'\right) = \begin{cases} 1, & x = x' \\ 0, & x \neq x' \end{cases} \tag{2}$$

In Eq. (1), Ω is the area of the integration containing x and x'. Since the Dirac delta function is used, this integral representation is exact providing $f(x)$ is defined and continuous in Ω. Then, the delta function is replaced by a smoothing function ($W\left(x - x', h\right)$) and the integral representation is

$$f(x) = \int_{\Omega} f(x')W\left(x - x', h\right)\mathrm{d}x' \tag{3}$$

where h is the smoothing length that defines the domain of influence of the smoothing kernel and $W(x - x', h)$ the kernel or smoothing function. While there are many kernel functions, this study uses the cubic spline one which has been widely used because it is similar to a Gaussian function which is considered the best choice as it is very stable and accurate but is not theoretically compact as it never goes to zero. Therefore, it will be computationally more expensive than other functions as a long distance is required for it to become practically close to zero. The

cubic spline function, which has the advantages of the Gaussian one and also compact support, has the form

$$W(q,h)=\alpha_d\begin{cases}1.5-q^2+0.5q^3 & 0\le q<1\\ \frac{(2-q)^3}{6} & 1\le q<2\\ 0 & q\ge 2\end{cases} \tag{4}$$

where $q=|x-x'|/h$ and $\alpha_d=\frac{1}{h},\frac{15}{7\pi h^2},\frac{3}{2\pi h^3}$ in one, two and three dimensions, respectively.

The next step is particle approximation which is represented as

$$f(x)=\sum_{j=1}^{N}\frac{m_j}{\rho_j}f(x_j)W\left(x-x_j,h\right) \tag{5}$$

with its derivative

$$\langle\nabla f(x)\rangle=\sum_{j=1}^{N}\frac{m_j}{\rho_j}f(x_j)\cdot\nabla_i W_{ij} \tag{6}$$

where

$$\nabla_i W_{ij}=\frac{x_i-x_j}{r_{ij}}\frac{\partial W_{ij}}{\partial r_{ij}} \tag{7}$$

where r_{ij} is the distance between particles i and j.

This SPH formulation is based on Navier–Stokes equations which state the conservation of mass, momentum and energy. If the Greek superscripts α and β denote the coordinate directions, that is, the repeated indices used for summation, these equations consist of the respective continuity and momentum ones.

$$\frac{\mathrm{D}\rho}{\mathrm{D}t}=-\rho\frac{\partial v^\beta}{\partial x^\beta} \tag{8}$$

$$\frac{\mathrm{D}v^\alpha}{\mathrm{D}t}=\frac{1}{\rho}\frac{\partial}{\partial x^\beta} \tag{9}$$

with their respective SPH formulations

$$\frac{\mathrm{D}\rho_i}{\mathrm{D}t}=\sum_{j=1}^{N}m_j v_{ij}^\beta\frac{\partial W_{ij}}{\partial x_i^\beta} \tag{10}$$

$$\frac{\mathrm{D}v_i^\alpha}{\mathrm{D}t}=\sum_{j=1}^{N}m_j\frac{\sigma_i^{\alpha\beta}+\sigma_j^{\alpha\beta}}{\rho_i\rho_j}\frac{\partial W_{ij}}{\partial x_i^\beta} \tag{11}$$

An additional dissipative term is added to the momentum equation to prevent any non-physical penetration and/or clumping of particles [37]. The most commonly used dissipation term is artificial viscosity and its mathematical formulations is

$$\prod_{ij}=\begin{cases}\frac{-\alpha_\Pi\bar{c}_{ij}\varnothing_{ij}+\beta\varnothing_{ij}^2}{\bar{\rho}_{ij}} & v_{ij}\cdot x_{ij}<0\\ 0 & v_{ij}\cdot x_{ij}\ge 0\end{cases} \tag{12}$$

$$\varnothing_{ij}=\frac{h_{ij}v_{ij}.x_{ij}}{\left|x_{ij}\right|^2+\varnothing^2} \tag{13}$$

$$\bar{c}_{ij}=\frac{1}{2}(c_i+c_j) \tag{14}$$

$$\bar{\rho}_{ij}=\frac{1}{2}(\rho_i+\rho_j) \tag{15}$$

$$h_{ij}=\frac{1}{2}(h_i+h_j) \tag{16}$$

$$v_{ij}=v_i-v_j, x_{ij}=x_i-x_j \tag{17}$$

To simulate the particles in a more orderly manner, an artificial compressibility technique called XSPH is introduced in the SPH formulation and, according to it, a particle moves in the following way.

$$\frac{\mathrm{d}x_i}{\mathrm{d}t}=v_i-\varepsilon\sum_j\frac{m_j}{\rho_j}v_{ij}W_{ij} \tag{18}$$

where ε is a constant in the range of 0–1.0. Using XSPH reduces the pressure fluctuations in a simulation which is a typical problem encountered with a weakly compressible SPH.

3 Constitutive law

Selecting the appropriate constitutive law is the core of any numerical tool. As elastic modeling in soil mechanics does not replicate a real soil's actual behavior, which is elasto-plastic under applied loads, the traditional elastic-solid model is not valid for geotechnical applications. Therefore, the elasto-plastic Drucker–Prager (D-P) model is chosen for the current study. As the stress tensor in the momentum equation requires a constitutive relationship, the detailed formation of a constitutive model is

$$\sigma^{\alpha\beta}=-p^{\alpha\beta}+s^{\alpha\beta} \tag{19}$$

where $\sigma^{\alpha\beta}$ is the total stress tensor, $\delta^{\alpha\beta}$ the Kronecher's delta, p the isotropic pressure and $s^{\alpha\beta}$ the deviatoric shear stress tensor.

The geomaterial is modeled as an elastic-perfectly plastic material with the definition of the strain rate ($\dot{\varepsilon}^{\alpha\beta}$)

$$\dot{\varepsilon}^{\alpha\beta} = \frac{1}{2}\left(\frac{\partial v^{\alpha}}{\partial x^{\beta}} + \frac{\partial v^{\beta}}{\partial x^{\alpha}}\right) \tag{20}$$

Which combines the elastic and plastic strain rates as

$$\dot{\varepsilon}^{\alpha\beta} = \dot{\varepsilon}_{e}^{\alpha\beta} + \dot{\varepsilon}_{p}^{\alpha\beta} \tag{21}$$

The elastic strain rate is calculated using the generalized Hooke's law as

$$\dot{\varepsilon}_{e}^{\alpha\beta} = \frac{\dot{s}'^{\alpha\beta}}{2G} + \frac{1-2\upsilon}{3E}\dot{\sigma}'^{\gamma\gamma}\delta^{\alpha\beta} \tag{22}$$

where $\dot{s}'^{\alpha\beta}$ is the deviatoric stress rate and $\dot{\sigma}'^{\gamma\gamma}$ the summation of the three components of the normal stress rate

$$s'^{\alpha\beta} = \sigma'^{\alpha\beta} - 1/3\sigma'^{\gamma\gamma}\delta^{\alpha\beta} \tag{23}$$

The plastic strain rate is computed using the plastic flow rule

$$\dot{\varepsilon}_{p}^{\alpha\beta} = \dot{\lambda}\frac{\partial g_{p}}{\partial \sigma'^{\alpha\beta}} \tag{24}$$

where $\dot{\lambda}$ is the rate of change in the plastic multiplier and g_p the plastic potential function that specifies the direction in which the plastic strain will develop. For non-associated type of flow rule, g_p does not coincide with the yield function (f) of the material and the value of λ can be determined by the consistency condition

$$\mathrm{d}f = \frac{\partial f}{\partial \sigma'^{\alpha\beta}} d\sigma'^{\alpha\beta} = 0 \tag{25}$$

Then, the total strain rate tensor is

$$\dot{\varepsilon}^{\alpha\beta} = \frac{\dot{s}'^{\alpha\beta}}{2G} + \frac{1-2\upsilon}{3E}\dot{\sigma}'^{\gamma\gamma}\delta^{\alpha\beta} + \dot{\lambda}\frac{\partial g_{p}}{\partial \sigma'^{\alpha\beta}} \tag{26}$$

Now, the general stress–strain relationship for an elastic-perfectly plastic material is

$$\frac{\mathrm{d}\sigma'^{\alpha\beta}}{\mathrm{d}t} = 2G\dot{e}^{\alpha\beta} + K\dot{e}^{\gamma\gamma}\delta^{\alpha\beta} - \dot{\lambda}\left[\left(K - \frac{2G}{3}\right)\frac{\partial g_{p}}{\partial^{mn}}\delta^{mn}\delta^{\alpha\beta} + 2G\frac{\partial g}{\partial \sigma^{\alpha\beta}}\right] \tag{27}$$

The yield criterion for the D-P model is expressed as

$$f\left(I_1, J_2\right) = \sqrt{J_2} + I_1\alpha_{\varnothing} - k_c = 0 \tag{28}$$

where I_1 and J_2 are the first and second invariants of the stress tensor, respectively, defined by

$$I_1 = \sigma'^{xx} + \sigma'^{yy} + \sigma'^{zz} \tag{29}$$

$$J_2 = \frac{1}{2}s'^{\alpha\beta}s'^{\alpha\beta} \tag{30}$$

and α_{φ} and k_c two D-P constants related to the soil cohesion (c) and frictional angle (φ) as

$$\alpha_{\varnothing} = \frac{\tan\varnothing}{\sqrt{9 + 12\tan^2\varnothing}} \tag{31}$$

$$k_c = \frac{3c}{\sqrt{9 + 12\tan^2\varnothing}} \tag{32}$$

The non-associated plastic flow rule is adopted, with the plastic potential function given by

$$g_p = \alpha_{\psi}I_1 + \sqrt{J_2} - \text{constant} \tag{33}$$

$$\alpha_{\psi} = \frac{\tan\psi}{\sqrt{9 + 12\tan^2\psi}} \tag{34}$$

The stress–strain relationship considering the Jaumann stress rate for the D-P model is

$$\frac{\mathrm{d}\sigma'^{\alpha\beta}}{\mathrm{d}t} = \sigma'^{\alpha\gamma}\dot{\omega}^{\beta\gamma} + \sigma'^{\gamma\beta}\dot{\omega}^{\alpha\gamma} + 2G\dot{e}^{\alpha\beta} + K\dot{e}^{\gamma\gamma}\delta^{\alpha\beta} - \dot{\lambda}\left[3K\alpha_{\psi}\delta^{\alpha\beta} + \frac{G}{\sqrt{J_2}}s'^{\alpha\beta}\right] \tag{35}$$

where

$$\dot{\lambda} = \frac{3\alpha_{\varnothing}K\dot{\varepsilon}^{\gamma\gamma} + \frac{G}{\sqrt{J_2}}\dot{s}^{\alpha\beta}\dot{\varepsilon}^{\alpha\beta}}{9\alpha_{\varnothing}K\alpha_{\psi} + G} \tag{36}$$

4 Soil–water two-phase model

The discussion in the previous section does not consider the effect of water particles in soil mechanics. As a coupled model can describe the real nature of a saturated soil well, a two-phase soil–water model is developed to simulate the interactions between water and soil, with a seepage force assumed. The water flowing through the pore space of the porous soil will exert a seepage force on the soil's structure and vice versa. The schematic layout of the two-phase model is depicted in Fig. 1 and the seepage flow estimated using the traditional soil mechanics formula

$$f = \gamma_{\mathrm{w}}n\frac{(v_{\mathrm{water}} - v_{\mathrm{soil}})}{k} \tag{37}$$

where γ_{w} is the unit weight of water, and n the porosity and k the co efficient of permeability of the soil. In this model, the momentum equation for soil is rewritten as

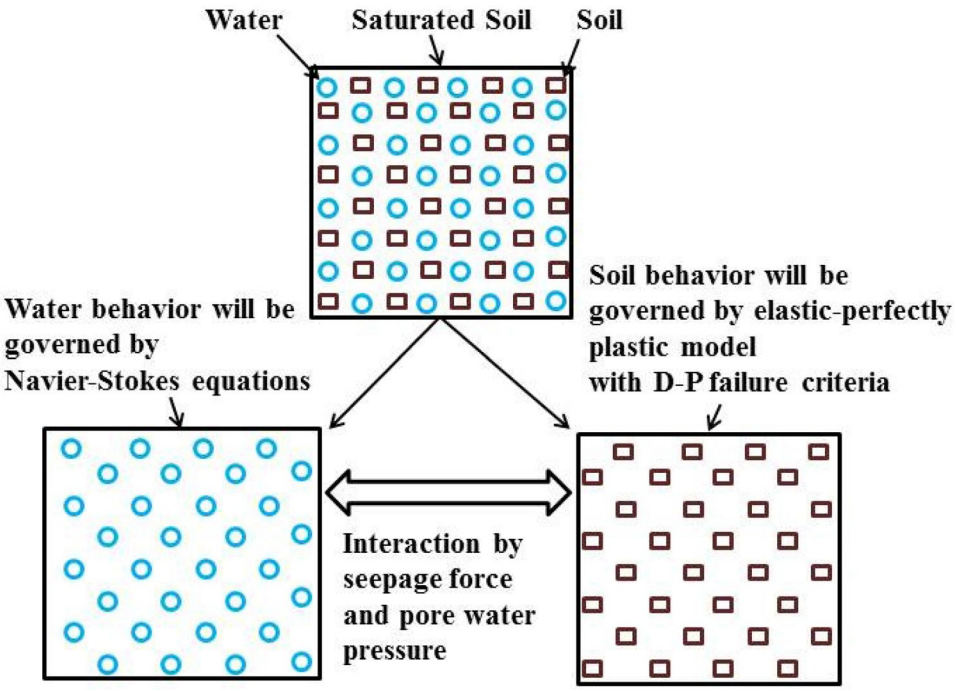

Fig. 1 Illustration of two-phase model

$$\frac{\mathrm{D}v_i^\alpha}{\mathrm{D}t} = \sum_{j=1}^{N} m_j \frac{\sigma_i' + \sigma_j'}{\rho_i \rho_j} \frac{\partial W_{ij}}{\partial x_i^\beta} - \prod_{ij} \delta^{\alpha\beta} + \sum_{j=1}^{N} m_j \frac{\gamma_w n \frac{(v_a - v_i)}{k}}{\rho_i \rho_a} W_{ia} - \sum_{j=1}^{N} \frac{m_j}{\rho_i \rho_j} (p_{wj} - p_{wi}) \frac{\partial W_{ij}}{\partial x_i^\alpha} + g_i^\alpha \tag{38}$$

where p_{wi} and p_{wj} are the pore water pressures on the respective soil particles.

The momentum equation for water is

$$\frac{\mathrm{D}v_a^\alpha}{\mathrm{D}t} = -\sum_{b=1}^{N} m_b \frac{p_a + p_b}{\rho_a \rho_b} \frac{\partial W_{ab}}{\partial x_a^\beta} + \sum_{b=1}^{N} m_b \frac{\mu_a \epsilon_a^{\alpha\beta} + \mu_b \epsilon_b^{\alpha\beta}}{\rho_a \rho_b} \frac{\partial W_{ab}}{\partial x_a^\beta} - \prod_{ab} \delta^{\alpha\beta} - \sum_{b=1}^{N} m_b \frac{\gamma_w n \frac{(v_a - v_i)}{k}}{\rho_i \rho_a} W_{ia} + g_a^\alpha \tag{39}$$

5 Validation of SPH model

As, prior to applying any developed tool, it is necessary to validate the model, following the general concept, three benchmark tests, simple shear, granular flow and permeability ones, were chosen for this purpose, with details of each provided in this section.

5.1 Simple shear test

A simple shear test is a very effective way of checking the accuracy of a model. For it, a soil layer of 30 cm × 30 cm was modeled in the SPH framework using a total of 900 particles, with a constant velocity applied to it to represent the simple shear condition. The parameters used in the simulation are summarized in Table 1. Measurements of the stress, strain and stress invariants were taken from the central area of the soil sample. The results of the simulation were compared with the analytical solution for the failure surface of D-P model, the initial and final configurations of which are shown in Fig. 2.

Table 1 Parameters used for simulation of simple shear test

Number of soil particles, *N*	900
Initial particle spacing (m), Δd	0.01
Smoothing length (m), h	0.012
Duration of a time step (s), Δt	0.00001
Density (kg/m^3), ρ	1800
Artificial viscosity parameter α,β	1.0
Modulus of elasticity (MPa), E	15
Poisson's ratio, v	0.35

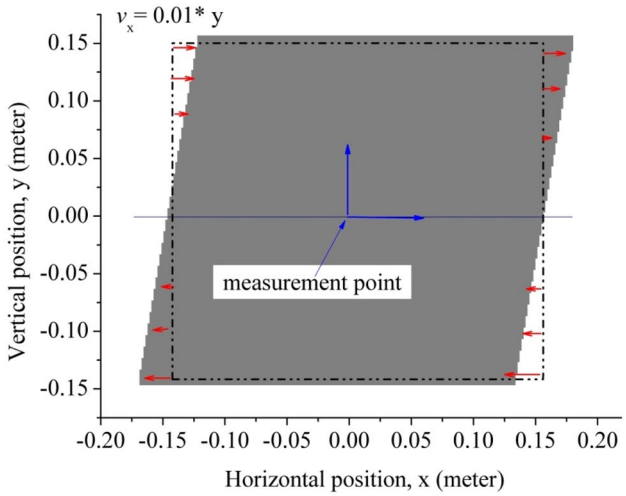

Fig. 2 Initial and deformed shapes obtained from simple shear test

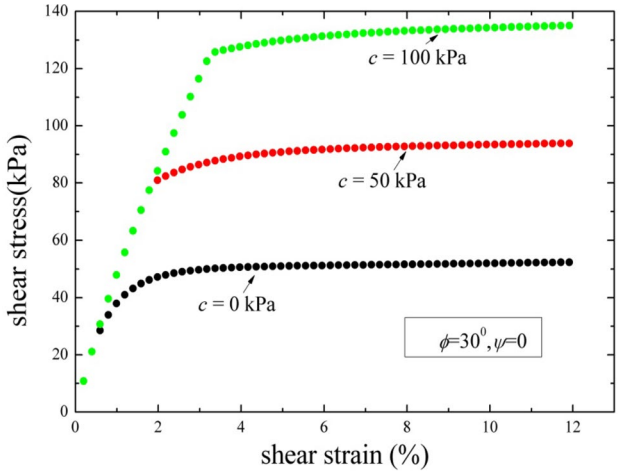

Fig. 4 Plots of shear stresses and strains for different cohesion values obtained from simple shear test by SPH

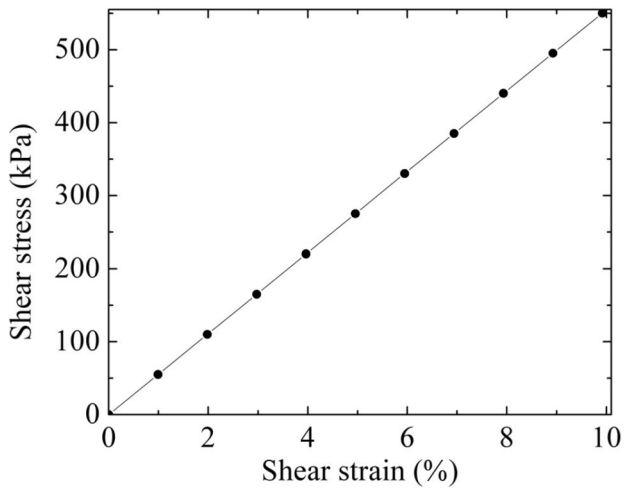

Fig. 3 Stress–strain relationship of elastic material obtained from simple shear test by SPH

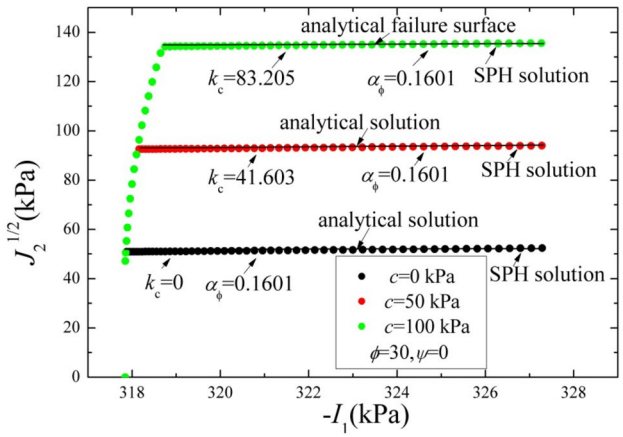

Fig. 5 Stress paths obtained from simple shear test by SPH

Figure 3 depicts the stress–strain relationship within the elastic range as linear, with the slope of the line the shear modulus (*G*) of the material which was found to be 5.55 MPa for the input parameters. Also, the stress–strain relationships for three different cohesion values are plotted in Fig. 4. It was determined that, with an increase in the cohesion value, the yield stress also increased and remained constant after reaching the failure surface. The stress paths for the same strength parameters are plotted in Fig. 5 and the failure surface obtained by SPH satisfactorily matched the analytical one. It was found that the D-P constants of this failure surface were exactly the same as those of the input values. As the results for different confining pressures also agreed well with the analytical solutions, overall, the SPH simulation successfully replicated the simple shear test.

5.2 Granular flow test

A typical granular flow was simulated to validate the numerical model developed. In it, exactly the same geometric and material properties of the benchmark experimental model [5] were used with an initial spacing of 0.0025 m. Its initial setup is shown in Fig. 6, and the parameters used in the simulation presented in Table 2. The failure surface of the broken column indicates a comprehensive similarity to the previous results, with the distributions of the progressive maximum shear strains at different times shown in Fig. 7. Although no data were available to check the progressive failure surface, it is clear that there were increases in the maximum shear strain.

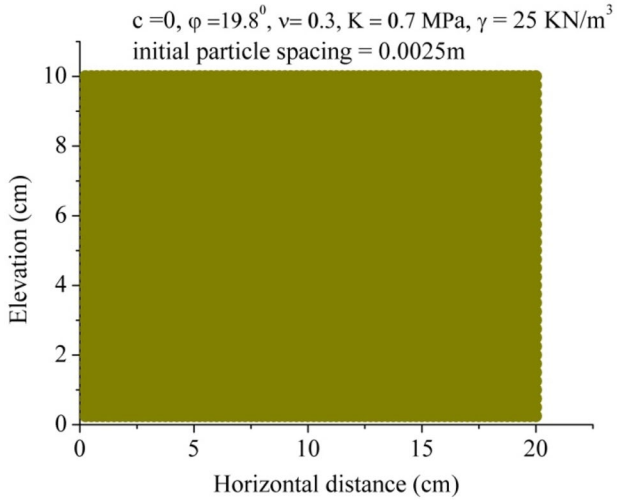

Fig. 6 Initial arrangements for SPH simulation of granular flow

Table 2 Parameters used in the simulation

Number of particles representing granular material, *N*	3200
Initial spacing (m), Δd	0.0025
Smoothing length (m), *h*	0.003
Duration of a time step (s), Δt	10^{-5}
Boundary type at horizontal base	Non-slip boundary
Boundary type at vertical wall	Symmetric boundary
Artificial viscosity parameter α,β	0.1

The flow pattern and flow surface coincide well with the experimental results provided in Bui et al. [5]

5.3 Falling head permeability test

The two-phase model was validated by simulating the conventional falling head permeability test. The head differences (*h*) at different time intervals were recorded and divided by the length of the soil sample (*L*) to obtain the hydraulic gradient (*i*) that is, $i = h/L$. The local velocity in the middle section of the soil sample was measured and multiplied by the porosity of the soil (*n*) to calculate the average velocity (*v*) that is, $v = v_{local}$ X *n*, with definitions of the terms provided in Fig. 8. By using Darcy's law, $k = v/i$ was determined and the values of *k* obtained from the simulation compared with the input ones, with the parameters used presented in Table 3. Figure 9 illustrates the relationship between the hydraulic gradients and average velocities obtained, with all the lines passing through the origin indicating that, if $h = 0$, there was no velocity. Figure 10 shows the *k* values determined through dividing the average velocity by the hydraulic gradient at different

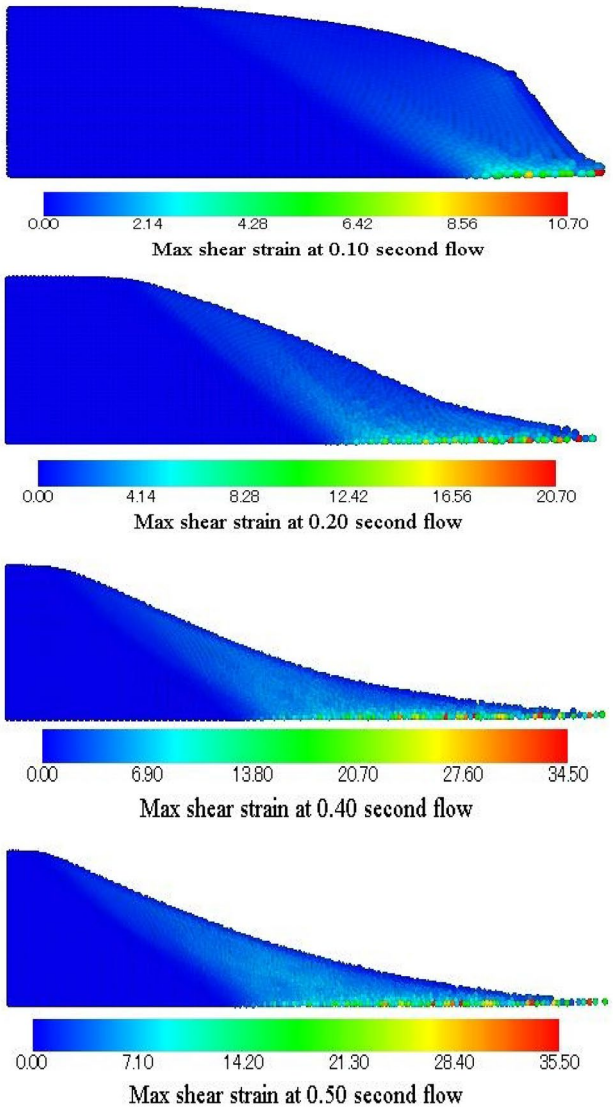

Fig. 7 Distributions of maximum shear strains for granular flows obtained by developed SPH code

times which were found to be stable during the entire simulation. A comparison of the average *k* values for the total time for each case and theoretical ones indicates that they matched well, as shown in Fig. 11

6 Geotechnical application of SPH method

6.1 Bearing capacity

Determining the bearing capacity of a soil is the primary concern of a practicing geotechnical engineer as the ultimate goal for any infrastructure is its capability to effectively transfer its load to the firm sub-soil for which

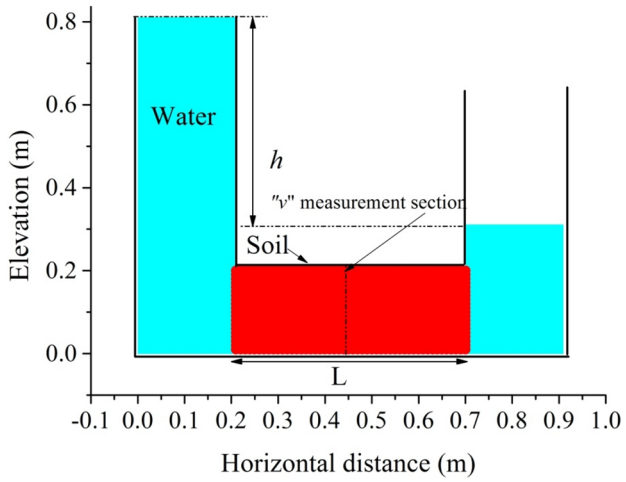

Fig. 8 Illustration of permeability test

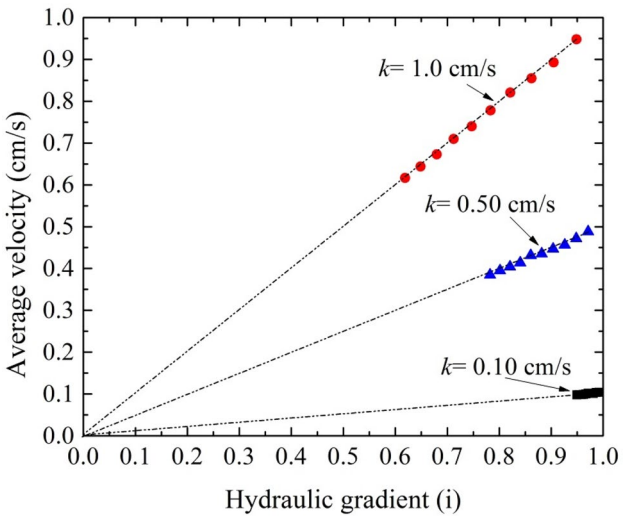

Fig. 9 Relationships of hydraulic gradients and average velocities obtained from simulation

Table 3 Summary of the parameters for the permeability test

Number of soil particles	1000
Number of water particles	3200
Initial particle spacing (m), Δd	0.01
Smoothing length (m)	0.012
Duration of a time step (s), Δt	5×10^{-5}
Density for soils (kg/m^3)	2008
Density for water (kg/m^3)	1000
Theoretical coefficient of permeability (cm/s), k	0.10, 0.50, 1.0
Porosity, n	0.40
Length of soil (cm), L	50
Initial water level difference (cm), h	50
Artificial viscosity parameter for water α,β	0.01, 0.01
Average velocity coefficient for water, ε	0.001
Boundary type at rigid base	Non-slip
Boundary type at vertical wall	symmetric

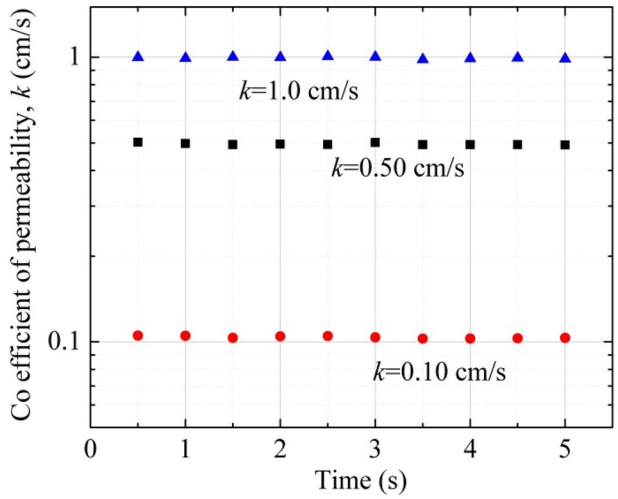

Fig. 10 k values obtained from simulation at different times

well-known theories are usually used. However, for a critical project and/or site with a complex geotechnical or structural profile, numerical modeling is required to analyze its bearing capacity. As discussed in the introduction, the settlement and punching of the foundation in a soil cannot be completely captured by traditional grid-based methods as it has been found that the final deformations in geotechnical projects were larger than those estimated [38]. Of the available grid-based methods, a FEM requires special care in order to avoid numerical problems whereas, in contrast, as a SPH one has no fixed connectivity between the particles, it is more suitable for problems related to penetration. This study focuses principally on the settlement and bearing capacity of clay and sand penetrated by a rigid foundation, and examines the formation of shear bands and stress-settlement behavior. To validate the model developed in the SPH framework, a typical bearing capacity analysis of a rigid footing allowed to settle into the soil layer at a constant rate was carried out. The mean stress below the footing was recorded with respect to the amount of settlement and the solution checked against the Prandtl one for the ultimate bearing capacity of cohesive material. The initial configuration for this analysis is shown in Fig. 12. The accumulation of shear strain was estimated from numerical simulations conducted at different times, and the results presented in Fig. 13 demonstrate the progressive settlement of the footing. The deformations caused by the penetration of a circular foundation into clay obtained from an experimental work conducted by

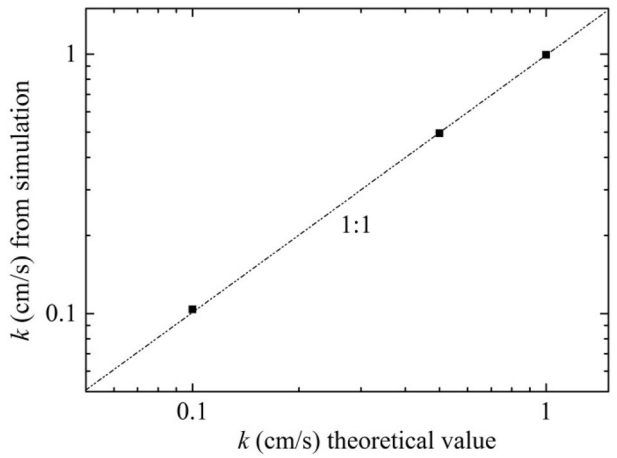

Fig. 11 Comparison of theoretical k values and those obtained from simulation

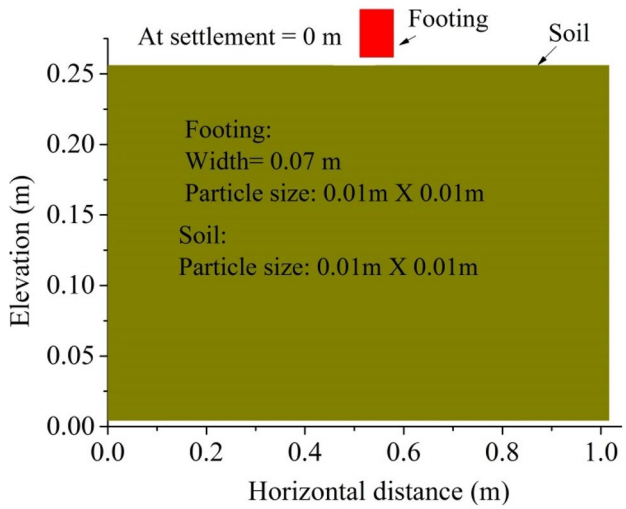

Fig. 12 Arrangement for bearing capacity test of cohesive soil using/by SPH

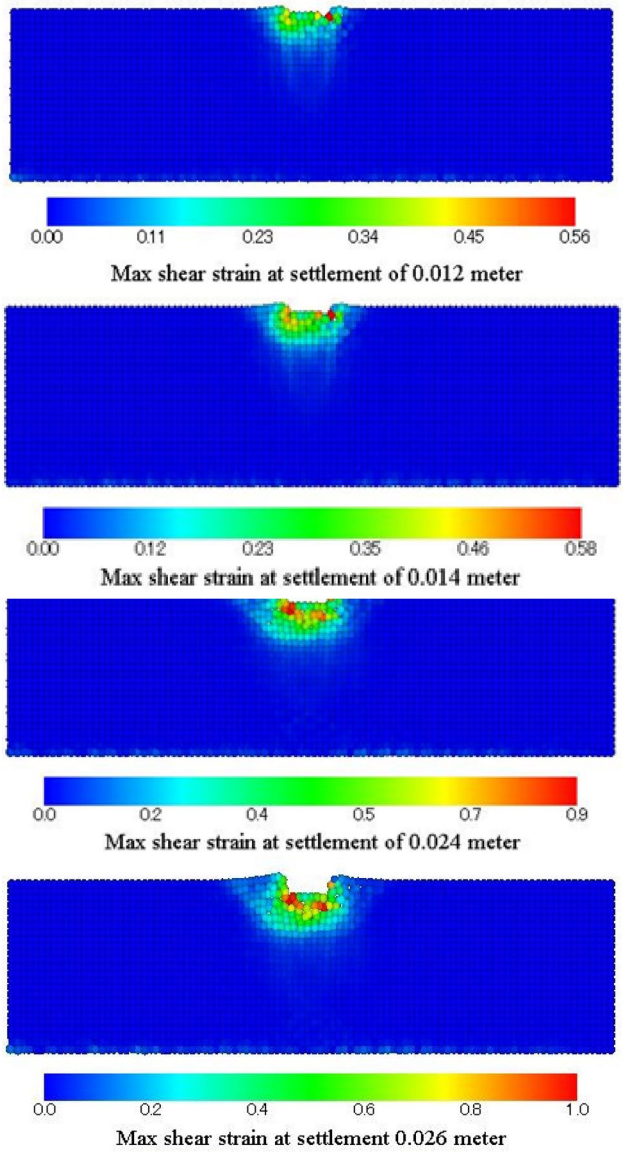

Fig. 13 Results obtained from SPH simulation of penetration of rigid footing in cohesive soil with $c = 30$ kPa

[39] and also reported in [38] are illustrated in Fig. 14. It can be seen that they were concentrated mainly under the foundation which was in good agreement with the pattern of those in Fig. 13. It was found that the failure surfaces were circular with radii approximately equal to the width of the footing, with that developed by the SPH code qualitatively justified. To further highlight the significance of the bearing capacity, the relationships between the footing's settlement and the pressure just below it for cohesive soils are plotted in Fig. 15. The Prandtl solution is somewhat compatible with FEM [40], and therefore, the comprehensive relationship between the analytical solution and SPH simulations implicitly justify the suitability of the described tools. The comparison of the SPH results and analytical solutions for a cohesive

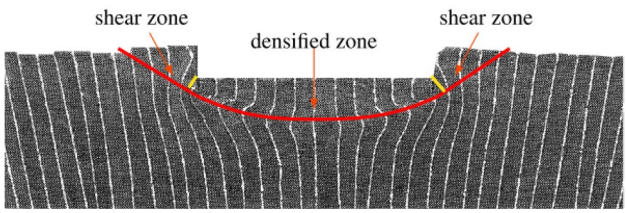

Fig. 14 Deformations of clay caused by penetration of circular foundation [38, 39]

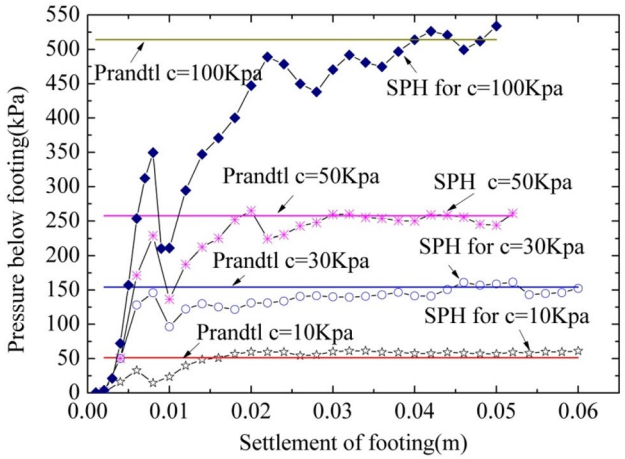

Fig. 15 Results obtained from bearing capacity test for different cohesion values

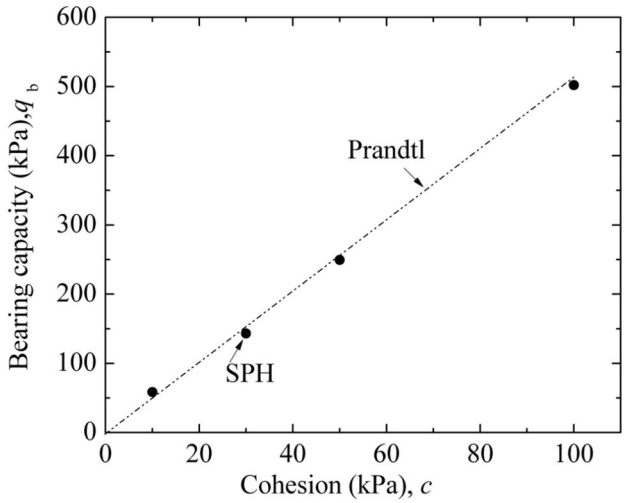

Fig. 16 Comparison of bearing capacity of cohesive soil determined by SPH and/with Prandtl

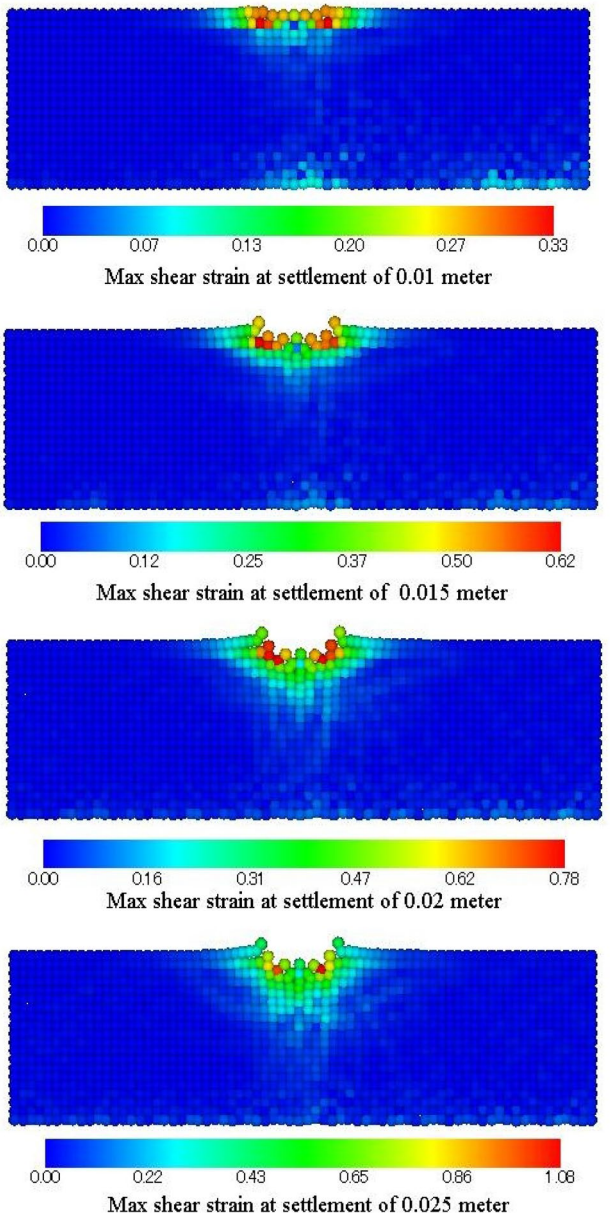

Fig. 17 Results obtained from SPH simulation of penetration of rigid footing in frictional soil with $\phi = 35°$

soil shown in Fig. 16 indicates that their ultimate bearing capacities matched satisfactorily.

Furthermore, a bearing capacity test of a frictional material was performed using the SPH code and its ultimate bearing capacity compared with that of the analytical solution. Figure 17 shows the deformation behaviors of the frictional material under the settlement of a rigid footing and the comparison in Fig. 18 demonstrates that their ultimate bearing capacities were a satisfactory match. Tables 4 and 5 summarize the parameters used in the simulation for bearing capacity for cohesive and cohesionless soil, respectively.

6.2 Seepage flow and boiling of soil

The seepage of ground water has often caused tragic failures of slopes and structures, for example, those of riverbanks, canals, embankments, coastal defenses and hillsides. According to [41], the seepage flow in the rubble mound beneath a caisson should be considered a significant influential factor in the design of a caisson type of composite breakwater for protecting against tsunamis. Another study [37] reveals that the seepage flow has a significant influence on the collapse of a breakwater

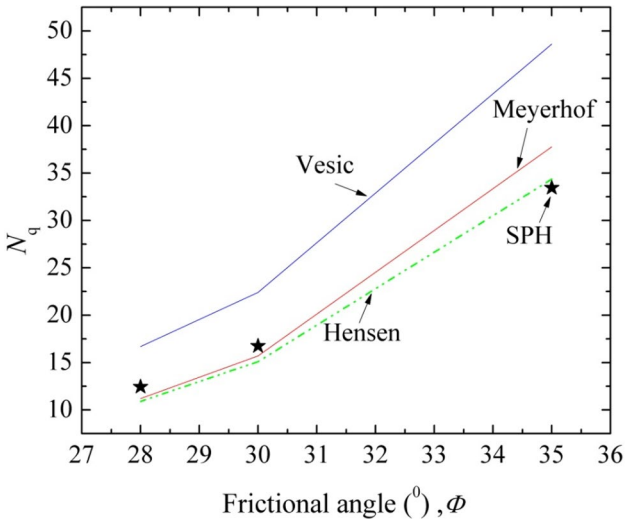

Fig. 18 Results obtained from bearing capacity test of frictional soils

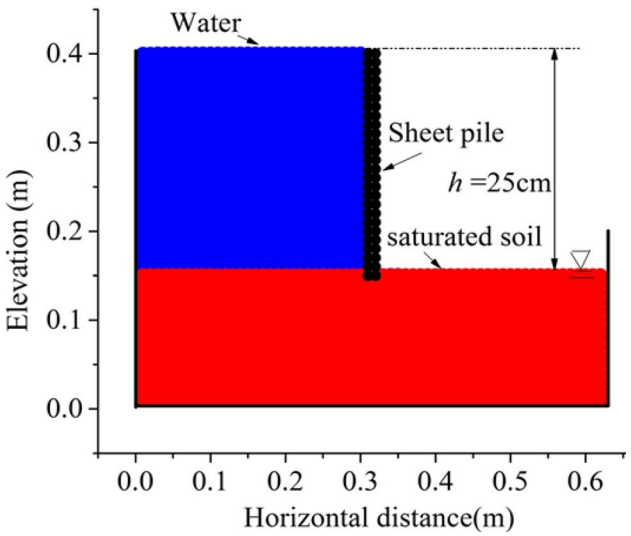

Fig. 19 Arrangement for seepage and boiling test

Table 4 Parameters used for SPH simulation of cohesive soil

Number of particles for soil, *N*	2500
Initial spacing (m), Δd	0.01
Gravity for cohesive material (m/s^2), *g*	0
Duration for a times step (s), Δt	10^{-5}
Boundary type at the rigid base	Non-slip boundary
Boundary type at the vertical walls	Symmetric boundary
Density of soil (kg/m3), ρ	1800
Cohesion values for cohesive soil (kPa), *c*	10, 15, 30, 50,100
Settlement rate of footing (m/s)	0.02
Width of footing (m), B_f	0.07

Table 5 Parameters used for SPH simulation of frictional soil

Number of particles for soil, *N*	1400
Initial spacing (m), Δd	0.01
Gravity for frictional material (m/s^2), *g*	9.81
Duration for a times step (s), Δt	10^{-5}
Boundary type at the rigid base	Non-slip boundary
Boundary type at the vertical walls	Symmetric boundary
Density of soil (kg/m3), ρ	1800
Frictional angle for frictional soil (degree), ϕ	35
Settlement rate of footing (m/s)	0.01
Width of footing (m), B_f	0.07

due to a tsunami wave. In the current research, a seepage flow is simulated to check the capability of the SPH code developed to reproduce a boiling phenomenon for a sheet-pile structure modeled as elastic materials with a high modulus of elasticity, as shown in Fig. 19, with Table 6 presenting a summary of the simulation's parameters. Figure 20 illustrates the progress of heave generation over time, Fig. 21 the velocity vector of water due to seepage flow and Fig. 22 the movements of soil particles in the form of the maximum strain due to the effect of the seepage force. It can be observed that the maximum area of strain is below the sheet pile, as is natural in a seepage flow.

Table 6 Parameters for seepage flow and boiling test

Number of soil particles	928
Number of water particles (initial)	1678
Initial particle spacing (m), Δd	0.01
Smoothing length (m)	0.012
Duration of a time step(s), Δt	2×10^{-5}
Density for soils (kg/m^3)	2008
Density for water (kg/m^3)	1000
Theoretical coefficient of permeability(cm/s), *k*	0.10
Porosity, *n*	0.50
Head difference (constant) (cm), *h*	25
Embedded depth of sheet pile (cm)	3
Thickness for sheet pile (cm)	2
Artificial viscosity parameter for soil α, β	0.1, 0.1
Artificial viscosity parameter for water α, β	0.001, 0
Average velocity coefficient for water, ε	0.30
Average velocity coefficient for water, ε	0.30
Boundary type at rigid base	Non-slip
Boundary type at vertical wall	Symmetric

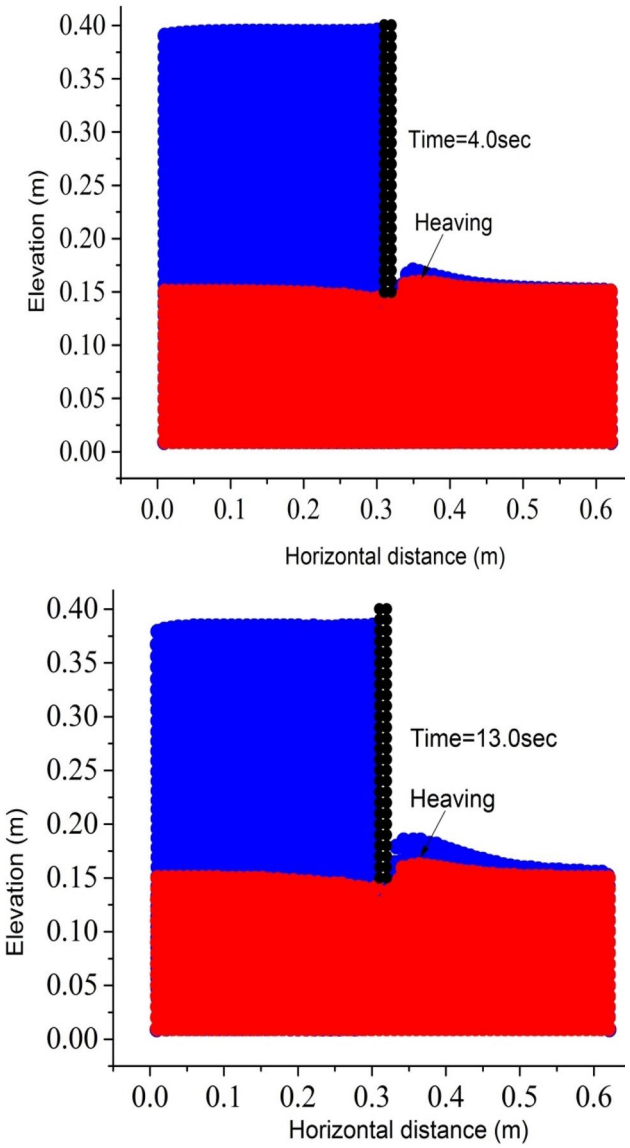

Fig. 20 Generations of heaving at different times

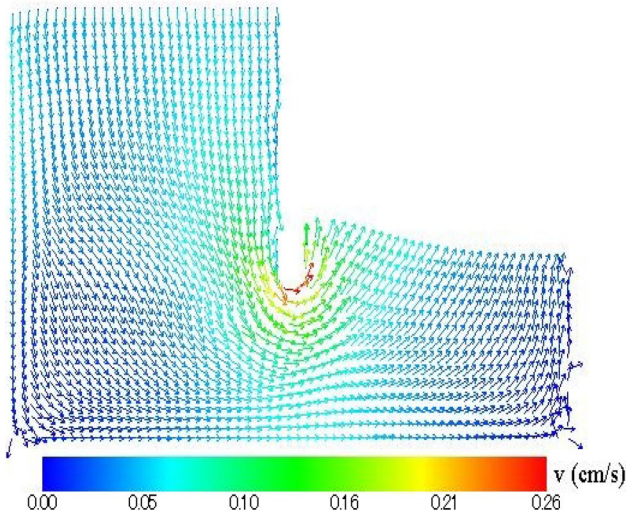

Fig. 21 Velocity vector of water at 13 s

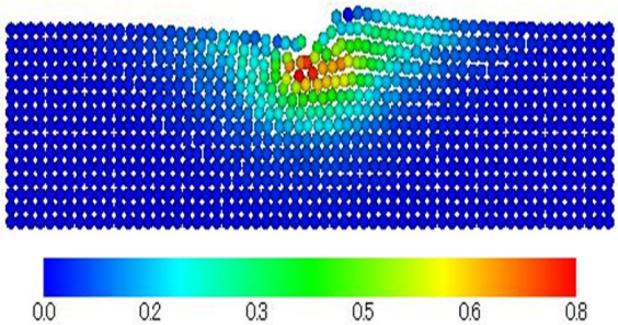

Fig. 22 Maximum shear strain distribution at 13 s

7 Conclusion

Simulating large deformations caused by the penetration of a rigid footing and the boiling effect of the seepage flow are perplexing tasks. In this study, the SPH method using an elastic–plastic constitutive model with the D-P failure criteria was applied to analyze the large deformations of geomaterials, as well as a water–soil coupled model to simulate saturated soil. Firstly, the simulation results obtained for two benchmark cases, a simple shear test and a granular flow one, were used to verify the developed code. Then, to validate the capability of the water–soil coupled model, a simulation of the seepage flow determined that it satisfied Darcy's law.

Simulations of the penetrations of a rigid footing into cohesive and frictional soils were performed. Comparisons of the simulated results and those obtained from existing analytical methods showed that they matched reasonably well for the bearing capacity below the footing. Finally, the boiling of soil was simulated and a great deal of the information obtained matched the conventional concept of the seepage flow and boiling phenomena. The study has also found that SPH does not require much computational time and can be simulated with commonly used processor. In future, work will expand this study to consider three-dimensional analyses and reproduce the real phenomena.

Compliance with ethical standards

Conflict of interest On behalf of all authors, the corresponding author states that there is no conflict of interest.

References

1. Huang Y, Dai Z (2014) Large deformation and failure simulations for geo-disasters using smoothed particle hydrodynamics method. Eng Geol 168:86–97. https://doi.org/10.1016/j.enggeo.2013.10.022
2. Liu GR, Liu MB (2003) Smoothed particle hydrodynamics a meshfree particle method. World Scientific Publishing, Singapore
3. Islam N, Hawlader B, Wang C, Soga K (2019) Large deformation finite-element modelling of earthquake-induced landslides considering strain-softening behavior of sensitive clay. Can Geotech J 56:1003–1018
4. Cundall PA, Strack ODL (1979) A discrete numerical model for granular assemblies. Geotechnique 29:47–65. https://doi.org/10.1680/geot.1979.29.1.47
5. Bui HH, Fukagawa R, Sako K, Ohno S (2008) Lagrangian meshfree particles method (SPH) for large deformation and failure flows of geomaterial using elastic–plastic soil constitutive model. Int J Numer Anal Methods Geomech 32:1537–1570. https://doi.org/10.1002/nag
6. Wang B, Vardon PJ, Hicks MA (2016) Investigation of retrogressive and progressive slope failure mechanisms using the material point method. Comput Geotech 78:88–98. https://doi.org/10.1016/j.compgeo.2016.04.016
7. Abe K, Soga K, Bandara S (2013) Material point method for coupled hydromechanical problems. J Geotech Geoenvironmental Eng 140:04013033. https://doi.org/10.1061/(asce)gt.1943-5606.0001011
8. Soga K, Alonso E, Yerro A et al (2017) Trends in large-deformation analysis of landslide mass movements with particular emphasis on the material point method. Géotechnique 68:457–458. https://doi.org/10.1680/jgeot.16.d.004
9. Lucy LB (1977) A numerical approach to the testing of the fission hypothesis. Astron J. https://doi.org/10.1086/112164
10. Rahman MA, Konagai K (2017) Substantiation of debris flow velocity from super-elevation: a numerical approach. Landslides 14:633–647. https://doi.org/10.1007/s10346-016-0725-3
11. Molteni D, Colagrossi A (2009) A simple procedure to improve the pressure evaluation in hydrodynamic context using the SPH. Comput Phys Commun 180:861–872. https://doi.org/10.1016/j.cpc.2008.12.004
12. Akbari H (2017) Simulation of wave overtopping using an improved SPH method. Coast Eng 126:51–68. https://doi.org/10.1016/j.coastaleng.2017.04.010
13. Dalrymple RA, Rogers BD (2006) Numerical modeling of water waves with the SPH method. Coast Eng 53:141–147. https://doi.org/10.1016/j.coastaleng.2005.10.004
14. Ferrari A (2010) SPH simulation of free surface flow over a sharp-crested weir. Adv Water Resour 33:270–276. https://doi.org/10.1016/j.advwatres.2009.12.005
15. Fang J, Owens RG, Tacher L, Parriaux A (2006) A numerical study of the SPH method for simulating transient viscoelastic free surface flows. J Nonnewton Fluid Mech 139:68–84. https://doi.org/10.1016/j.jnnfm.2006.07.004
16. Crespo AJ, Gómez-Gesteira M, Dalrymple RA (2008) Modeling dam break behavior over a wet bed by a SPH Technique. J Waterw Port, Coastal, Ocean Eng 134:313–320. https://doi.org/10.1061/(asce)0733-950x(2008)134:6(313)
17. Ran Q, Tong J, Shao S et al (2015) Advances in water resources incompressible SPH scour model for movable bed dam break flows. Adv Water Resour 82:39–50. https://doi.org/10.1016/j.advwatres.2015.04.009
18. Gholami Korzani M, Galindo-Torres SA, Scheuermann A, Williams DJ (2018) SPH approach for simulating hydro-mechanical processes with large deformations and variable permeabilities. Acta Geotech 13:303–316. https://doi.org/10.1007/s11440-017-0610-9
19. Peng C, Wu W, Yu H, Sui, Wang C, (2015) A SPH approach for large deformation analysis with hypoplastic constitutive model. Acta Geotech 10:703–717. https://doi.org/10.1007/s11440-015-0399-3
20. Ghaïtanellis A, Violeau D, Ferrand M et al (2018) A SPH elastic-viscoplastic model for granular flows and bed-load transport. Adv Water Resour 111:156–173. https://doi.org/10.1016/j.advwatres.2017.11.007
21. Shadloo MS, Oger G, Le Touzé D (2016) Smoothed particle hydrodynamics method for fluid flows, towards industrial applications: motivations, current state, and challenges. Comput Fluids 136:11–34. https://doi.org/10.1016/j.compfluid.2016.05.029
22. Chang TJ, Kao HM, Chang KH, Hsu MH (2011) Numerical simulation of shallow-water dam break flows in open channels using smoothed particle hydrodynamics. J Hydrol 408:78–90. https://doi.org/10.1016/j.jhydrol.2011.07.023
23. Zhang W, Maeda K (2015) Numerical Simulations of Slope and Levee Failure under heavy rainfall using the three-phase SPH Model. J Japan Soc Civ Eng Ser A2 Applied Mech 70:I_483-I_494. https://doi.org/10.2208/jscejam.70.i_483
24. Liang H, He S, Liu W (2019) Dynamic simulation of rockslide-debris flow based on an elastic–plastic framework using the SPH method. Bull Eng Geol Environ. https://doi.org/10.1007/s10064-019-01537-8
25. An Y, Wu Q, Shi C, LIU Q, (2016) Three-dimensional smoothed-particle hydrodynamics simulation of deformation characteristics in slope failure. Géotechnique 66:670–680. https://doi.org/10.1680/jgeot.15.p.222
26. Reyes Y, Roose D, Recarey Morfa C (2012) Dynamic refinement for SPH simulations of post-failure flow of non-cohesive soil. Proc 7th Int SPHERIC Work 71–77
27. Li L, Rao X, Amini F, Tang H (2015) SPH modeling of hydraulics and erosion of HPTRM levee. J Adv Res Ocean Eng 1:1–13. https://doi.org/10.5574/jaroe.2015.1.1.001
28. Huang Y, Zhang W, Mao W, Jin C (2011) Flow analysis of liquefied soils based on smoothed particle hydrodynamics. Nat Hazards 59:1547–1560. https://doi.org/10.1007/s11069-011-9851-3
29. Bui HH, Fukagawa R, Sako K, Wells JC (2008) SPH-based numerical simulations for large deformation of geomaterial considering soil-structure interaction. 12th Int Conf Int Assoc Comput Methods Adv Geomech 1:570–578
30. Khanpour M, Zarrati AR, Kolahdoozan M et al (2016) Mesh-free SPH modeling of sediment scouring and flushing. Comput Fluids 129:67–78. https://doi.org/10.1016/j.compfluid.2016.02.005
31. Chen W, Qiu T (2014) Simulation of earthquake-induced slope deformation using SPH. Int J Numer Anal Methods Geomech 38:297–330. https://doi.org/10.1002/nag
32. Gholami Korzani M, Galindo-Torres SA, Scheuermann A, Williams DJ (2018) Smoothed Particle Hydrodynamics for investigating hydraulic and mechanical behaviour of an embankment under action of flooding and overburden loads. Comput Geotech 94:31–45. https://doi.org/10.1016/j.compgeo.2017.08.014
33. Braun A, Cuomo S, Petrosino S et al (2018) Numerical SPH analysis of debris flow run-out and related river damming scenarios for a local case study in SW China. Landslides 15:535–550. https://doi.org/10.1007/s10346-017-0885-9
34. Zhu C, Huang Y, Zhan L, Tong (2018) SPH-based simulation of flow process of a landslide at Hongao landfill in China. Nat Hazards 93:1113–1126. https://doi.org/10.1007/s11069-018-3342-8
35. Huang Y, Cheng H, Dai Z et al (2015) SPH-based numerical simulation of catastrophic debris flows after the 2008 Wenchuan earthquake. Bull Eng Geol Environ 74:1137–1151. https://doi.org/10.1007/s10064-014-0705-6

36. Huang Y, Dai Z, Zhang W, Chen Z (2011) Visual simulation of landslide fluidized movement based on smoothed particle hydrodynamics. Nat Hazards 59:1225–1238. https://doi.org/10.1007/s11069-011-9859-8
37. Islam MR, Hayano K, Rahman MA (2019) Insights into effects of seepage on failure of breakwater mound: experimental and numerical investigations. Indian Geotech J. https://doi.org/10.1007/s40098-019-00356-8
38. Schneider-Muntau B, Bathaeian I (2018) Simulation of settlement and bearing capacity of shallow foundations with soft particle code (SPARC) and FE. GEM - Int J Geomathematics 9:359–375. https://doi.org/10.1007/s13137-018-0109-z
39. Tani K, Craig WH (1995) Bearing capacity of circular foundations on soft clay of strength increasing with depth. Soils Found 35:21–35
40. Chen EWF, Mizuno E (1990) Nonlinear analysis in soil mechanics. Elsevier Science
41. Dong S, Zen K, Kasama K, Wang B, Takesue A (2012) Theoretical and experimental study on tsunami induced instability of caisson type composite breakwater. Mem Fac Eng Kyushu Univ 72(2):55–68